

Supplementary Information for: Reentrant superconductivity and superconductor-to-insulator transition in a naturally occurring Josephson junction array tuned by RF power

S. Avraham, S. Sankar, S. Sandik, A. Burshtein, M. Goldstein, E. Sela, and Y. Dagan*

School of Physics and Astronomy, Tel Aviv University, Tel Aviv 6997801, Israel

(Dated: June 25, 2025)

I. THE BLOCH BAND PICTURE

As noted in the main text, the zero-bias peak R_I in Fig. 1a of the main text cannot be captured within the RCSJ model. We speculate that its emergence may be attributed to the dual Bloch band picture. The periodic potential of a Josephson junction, $-E_J \cos \phi$, gives rise to Bloch wavefunctions that are 2π -periodic in ϕ up to a phase that depends on the quasicharge q , which is analogous to the crystal momentum k in solid state systems and is defined in the Brillouin zone $-e \leq q \leq e$. From the solid state analogy, we find energy bands $E_n(q)$ that depend periodically on q and are given by the Mathieu characteristic values [1], where $n = 0, 1, \dots$ is the band index. In the experimentally-relevant limit $E_J \gg E_C$, the junction potential is in the tight-binding limit, and the lowest Bloch band is approximately given by $E_0(q) \approx -\Delta \cos(\pi q/e)$, where $\Delta \approx \frac{32}{2^{1/4}\sqrt{\pi}}(E_J^3 E_C)^{1/4} e^{-\sqrt{8E_J/E_C}}$ is the phase slips rate, which is the tunneling amplitude between adjacent minima in the cosine potential.

The superconducting phase ϕ and the quasicharge q are conjugate variables and satisfy an uncertainty relation. If the quantum fluctuations in the quasicharge are small (corresponding to a fluctuating phase), the semiclassical equation of motion for a junction biased by DC and RF currents $I_{b,RF}$ reads [2]

$$\dot{q} = -\frac{1}{R_{qp}} \frac{dE_0(q)}{dq} + I_b + I_{RF} \sin(\omega_{RF} t), \quad (\text{S1})$$

where R_{qp} is the quasiparticle resistance of the junction and $\omega_{RF} = 2\pi f_{RF}$. Here we assume that the bias currents and the temperature are small enough such that the quasicharge is restricted to the lowest Bloch band, $n = 0$. This equation is dual to the RCSJ equation (Eq. (1) of the main text), with the absence of a second-derivative inertia term \ddot{q} ; this term may be added with an inductor L connected in series with the junction (dual to the parallel capacitance in the RCSJ model), but is unimportant in the following discussion and we omit it henceforth.

The analysis of Eq. (S1) is due to Likharev and Zorin [2]. Consider the case $I_{RF} = 0$, and set $E_0(q) \approx -\Delta \cos(\pi q/e)$. At $I_b < I_{th}$ with $I_{th} = \pi\Delta/(eR_{qp})$, the solution for the quasicharge is stationary, $\dot{q} = 0$, and the current flows through the quasiparticle channel, such that the voltage across the junction is $V = I_b R_{qp}$. As I_b exceeds the threshold I_{th} , the quasicharge is no longer stationary and enters the Bloch oscillations regime, less current flows through the quasiparticle channel, and the differential resistance dV/dI_b is negative. One therefore expects a resistance peak around $I_b = 0$ with a width I_{th} . Such a peak was observed for resistively-shunted junctions [3], and also for a two-dimensional Josephson array [4].

Let us now consider the effect of a small RF current on the resistance peak. Within linear response in I_{RF} , we write $q(t) = \tilde{q}(t) + \Re\{\delta q e^{i\omega_{RF} t}\}$, where $\tilde{q}(t)$ is the solution to Eq. (S1) in the absence of RF current. Plugging $q(t)$ to Eq. (S1) and expanding in $\delta q/\tilde{q} \ll 1$, we find

$$\delta q = \frac{I_{RF}}{\omega_{RF} + i \frac{\pi^2 \Delta}{e^2 R_{qp}} \cos(\pi \tilde{q}/e)}. \quad (\text{S2})$$

The correction δq renormalizes the Bloch bandwidth Δ . To see this, plug $q = \tilde{q} + \Re\{\delta q e^{i\omega_{RF} t}\}$ into $\Delta \sin(\pi q(t)/e)$:

$$\Delta \sin(\pi q(t)/e) = \Delta J_0(\pi|\delta q|/e) \times \sin(\pi \tilde{q}/e) + \sum_{n \neq 0} J_n(\pi|\delta q|/e) e^{in(\omega_{RF} t - \varphi)}, \quad (\text{S3})$$

where $J_n(x)$ is the n th Bessel function of the first kind, and φ is the phase of δq . Integrating over a period of the RF current, the high-order Bessel functions average out, and we are left with a renormalized DC term:

$$\Delta_{\text{eff}} = \Delta J_0(\pi|\delta q|/e). \quad (\text{S4})$$

* Corresponding author: yodagan@tauex.tau.ac.il

Using $J_0(x \ll 1) \approx 1 - x^2/4$, we find that Δ_{eff} is reduced as the RF current is increased. This effect is expected to diminish at large frequencies, $\omega_{\text{RF}} \gg \pi^2\Delta/(e^2R_{\text{qp}})$. We note that the same conclusions may be derived by diagonalizing the Floquet Hamiltonian of a periodically-tilted cosine potential and extracting the width of the lowest Bloch band from the Floquet quasienergies [5]. Recalling that the Bloch bandwidth Δ is the tunneling rate in the cosine potential, this effect may be interpreted as the coherent destruction of tunneling [6].

In the experiment, the zero-bias resistance peak narrows as the RF power is increased, as shown in Fig. 1a of the main text. This is in line with the prediction of the Bloch band picture: decreasing Δ_{eff} corresponds to decreasing $I_{\text{th}} = \pi\Delta_{\text{eff}}/(eR_{\text{qp}})$. However, the rest of Fig. 1a is captured quite well by the RCSJ model, which cannot coexist with the Bloch band picture, since the two models correspond to two different regimes of quantum fluctuations in ϕ and q . This possibly suggests that a more complete analysis is required to explain the experimental observations, not only the low-temperature phase diagram, but also the reentrant superconductivity at finite temperatures.

II. CONTROLLING E_J WITH RF CURRENT

In this section, we demonstrate how the application of RF current leads to a reduction in E_J within the RCSJ picture. Consider the semiclassical equation of motion for the phase,

$$\frac{\phi_0}{2\pi}C\ddot{\phi} + \frac{\phi_0}{2\pi R}\dot{\phi} + I_c \sin(\phi) = I_b + I_{\text{RF}} \sin(\omega_{\text{RF}}t). \quad (\text{S5})$$

Note that now R is the normal state resistance of the junction and not the quasiparticle resistance in the Bloch band picture. Neglecting the capacitive inertia term, which is unimportant in this context, the equation for the phase ϕ is dual to Eq. (S1) for the charge, with the critical current I_c replacing the phase slips rate Δ . One may repeat the calculation from the previous section in the present situation: applying linear response in the RF current leads to a renormalization of the critical current,

$$\delta I_{c,\text{eff}} = I_c J_0(|\delta\phi|), \quad (\text{S6})$$

with

$$\delta\phi = \frac{RI_{\text{RF}}}{\frac{\phi_0}{2\pi}\omega_{\text{RF}} + iRI_c \cos(\tilde{\phi})}, \quad (\text{S7})$$

where $\tilde{\phi}$ is the solution to Eq. (S5) at $I_{\text{RF}} = 0$. Thus, we find that $E_{J,\text{eff}} = \Phi_0 I_{c,\text{eff}}/(2\pi)$ decreases as I_{RF} increases.

Note that Eqs. (S4) and (S6) result from the Bloch band and RCSJ pictures, respectively, which correspond to different regimes of quantum fluctuations and hint at a non-trivial dependence of the junction parameters on the RF current. On the one hand, the Bloch band picture predicts that the phase slips rate is decreased as the RF current is increased. On the other hand, the RCSJ model predicts a decrease in I_c and hence E_J as well, corresponding to a larger phase slips rate $\Delta \sim e^{-\sqrt{8E_J/E_C}}$. We conclude that the dependence of the junction parameters on the RF current is drastically altered by the regime of quantum fluctuations.

III. COMPARING THE EXPERIMENT WITH THE RCSJ MODEL

In a simplified picture, the granular aluminum (grAl) sample can be thought of as a stack of many parallel 1D JJ chains. When current biased, the currents flowing through the parallel chains would be roughly the same since the long 1D chains are statistically similar. The individual JJs in the 1D chain are modeled as RCSJ junctions and so the 1D chain consists of RCSJ junctions in series. In the current bias case, the dynamics of the individual RCSJ junctions decouple with the individual dynamics described by Eq. (1) in the main text. The total voltage across the chain is simply the sum of voltages across the individual junctions. The RCSJ parameters $\Omega = \phi_0 f_{\text{RF}}/(I_c R)$, $\beta = 2\pi R^2 C I_c/\phi_0$ of the individual junctions are expected to be very similar with some mean value and a small variance; the small variance is expected to result in smoothening of sharp features such as the Shapiro steps [7]. We attempt to estimate the RCSJ parameters (mean value) for the experimental system.

We can estimate Ω directly from Fig. 1a of the main text, where the RF drive is at frequency $f_{\text{RF}} = 24.5$ MHz. The number of steps, N_s , that would occur for a given range of the normalized DC current, δi , is determined by Ω : $N_s \sim \delta i/\Omega$. In the figure we can see around 3 steps between $I_b = 0$ and $I_b = 1 \mu\text{A}$. Then, using the zero-temperature critical current value for the sample (see Fig. 2c in the main text), $I_{c,\text{tot}} \sim 7 \mu\text{A}$, we get $\Omega \sim 0.05$. Now, let us calculate Ω using its defining relation, $\Omega = \phi_0 f_{\text{RF}}/(I_c R)$. Let N_c denote the number of parallel chains and N denote

the number of RCSJ junctions in a chain. At large current bias, all the RCSJ junctions become purely ohmic, and then the total voltage across the sample is simply given by, $V = NRI_b/N_c$. From the frequency dependence of the giant Shapiro steps, we find $N = 430$ in the main text. The critical current of an RCSJ junction is related to the total critical current of the sample by, $I_c = I_{c,\text{tot}}/N_c$. Then we get,

$$I_c R = \frac{I_{c,\text{tot}}}{N} \frac{V}{I_b}, \quad \text{for large } I_b. \quad (\text{S8})$$

The sample resistance at large bias is $V/I_b \sim 1 \text{ k}\Omega$. Then, plugging in the value of $I_{c,\text{tot}}$ and N , we get, $I_c R \sim 0.01 \text{ mV}$ and consequently $\Omega \sim 0.005$. This estimate is one order of magnitude smaller than the directly estimated Ω from Fig. 1a. The origin of this discrepancy is not fully clear. One possible cause could be that the superconducting coherence length $\sim 10 \text{ nm}$ is greater than the grain size, and this could result in multiple grains combining to form an effective RCSJ junction. In that case, the factor $N = 430$ reported in the main text would correspond to the number of such effective RCSJ junctions in series. But in the fully ohmic regime at large I_b , the resistance between the grains would come into play and this could be seen to effectively increase N in Eq. S8, which consequently would decrease $I_c R$ and thereby increase Ω . Thus we believe that the estimate $\Omega \sim 0.005$ calculated from its defining relation should only be a lower bound.

The direct estimation of the parameter β for the RCSJ junctions is complicated since the capacitance C would depend on various factors. We attempt to qualitatively infer β . If $\beta \ll 1$, then in this overdamped case, the Shapiro steps should extend much above the critical current, unlike in the experiment. On the other hand, if $\beta \gg 1$, then the Shapiro steps would be hardly visible. Both these features could be seen in Fig. S1. Based on these considerations we believe that $\beta \sim 1$ in our case. Next, using the relation $\beta\Omega = 2\pi RC f_{\text{RF}}$, and using the inferred $\Omega \sim 0.05$ and $R \sim 2 \text{ k}\Omega$ (assuming, $N_c = N_y \times N_z$, we get $I_c \sim 5 \text{ nA}$ and then from $I_c R \sim 0.01 \text{ mV}$, we get R), we get $C \sim 100 \text{ fF}$. We then see that $E_J/E_c \sim 10$. This large E_J/E_c ratio is consistent with the fact that at low RF powers, the sample is superconducting.

IV. PHENOMENOLOGICAL EXPLORATION OF REENTRANT SUPERCONDUCTIVITY USING THE RCSJ MODEL

In the main text, we attribute the reentrance of superconductivity to a decrease of the charging energy E_C with temperature T via the mechanism discussed in Ref. [8]. The Efetov model predicts reentrance from an insulating phase to a superconducting phase; here we phenomenologically explore the possibility of reentrance using the RCSJ model, which cannot capture the insulating state. We phenomenologically show that reentrance from a normal phase to a superconducting phase is possible, by assuming that the primary effect of increasing T is to reduce E_C and E_J . The reduction of E_C and E_J leads to the reduction of the plasma frequency $\omega_p \sim \sqrt{E_J E_C}$. To study the physics associated with the reduction of ω_p , it is better to express the RCSJ equation in a dimensionless form where the drive frequency is scaled by the plasma frequency. This is done using the dimensionless time coordinate $\tau = \omega_p t$ in Eq. S5 to get,

$$\partial_\tau^2 \phi + \sigma \partial_\tau \phi + \sin \phi = i_0 + i_1 \sin \tilde{\Omega} \tau. \quad (\text{S9})$$

Here $i_0 = I_b/I_c$ and $i_1 = I_{\text{RF}}/I_c$ are the scaled currents. The parameter σ is the damping parameter and is related to the parameter β in the Stewart-McCumber form by $\sigma = 1/\sqrt{\beta}$. The frequency $\tilde{\Omega}$ is scaled by the plasma frequency, i.e. $\tilde{\Omega} = \omega/\omega_p$; $\tilde{\Omega}$ is related to the Ω in the Stewart-McCumber form by $\tilde{\Omega} = \Omega/\sigma$.

For simplicity, we assume a linear reduction of I_c with T . The exact nature of how E_C changes with T is not known. For the purpose of exploring what magnitude of change in E_C is required for reentrance to occur in the RCSJ description, we consider an abrupt change in E_C after some $T^* < T_c$. This would result in $\sigma = \sigma_0$ at $T < T^*$ going to $\sigma = \sigma_1$ at $T > T^*$. Note that the corresponding change in $\tilde{\Omega}$ follows from its relation to Ω . We choose $\sigma_0 = 1$ and $\tilde{\Omega} = 0.03$ (corresponding to $\beta = 1$ and $\Omega = 0.03$) at $T = 0$, which are close to the parameters estimated in the previous section. We also choose $T^* = 0.8T_c$. The effect of σ_1 on reentrance is explored in Fig. S2. A crude qualitative resemblance to the experimental results in Fig. 1b and Fig. 2a is seen. However, we reiterate that the feature associated with the strong insulator is not captured, as it is beyond the scope of the RCSJ description. From the results, we find that $\sigma_1 \lesssim 0.1\sigma_0$ is required for reentrance. Thus E_C should decrease by around 3 orders of magnitude for the reentrance to occur within the RCSJ description for the estimated parameter regime of the experiment.

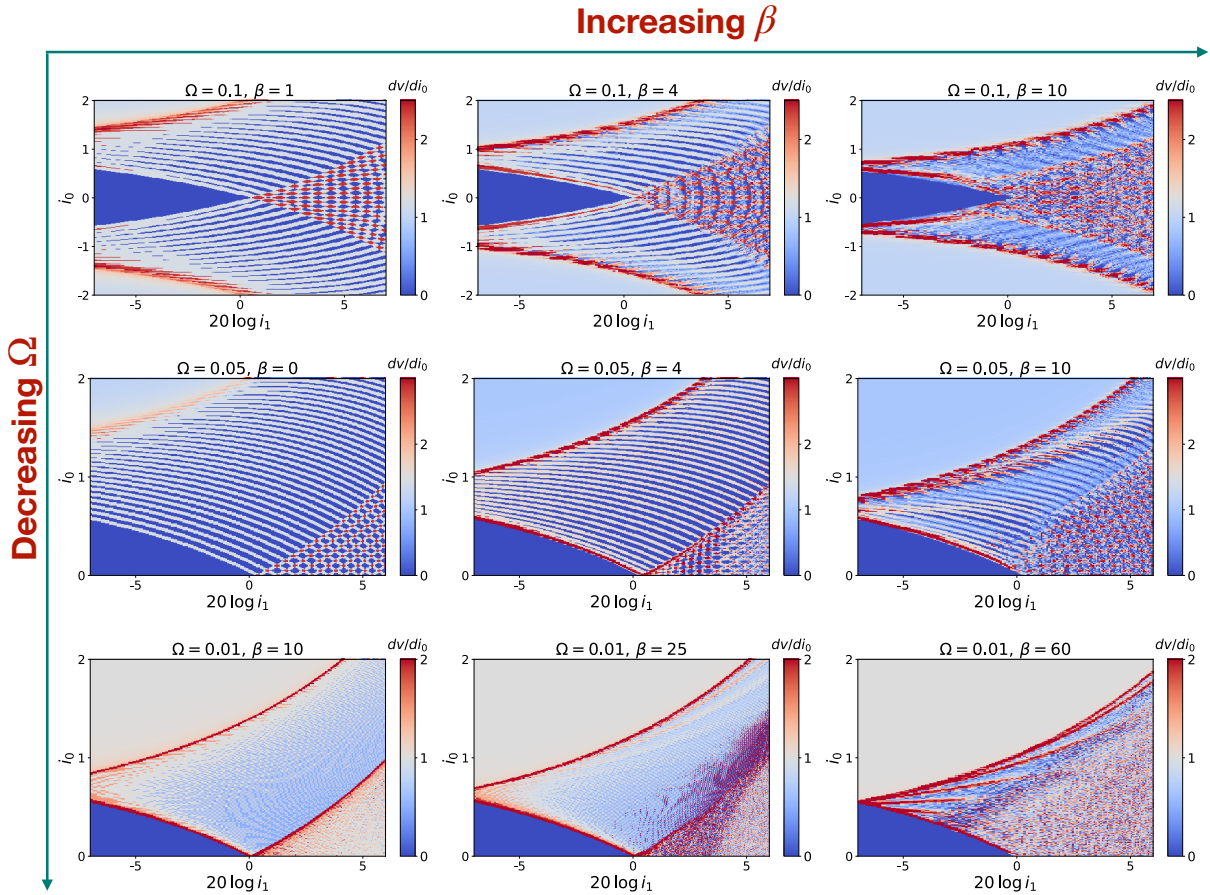


FIG. S1: Survey of Shapiro maps obtained from the RCSJ model in the $\beta - \Omega$ parameter space. For the cases starting from the second row, only half of the map is calculated to reduce calculation time.

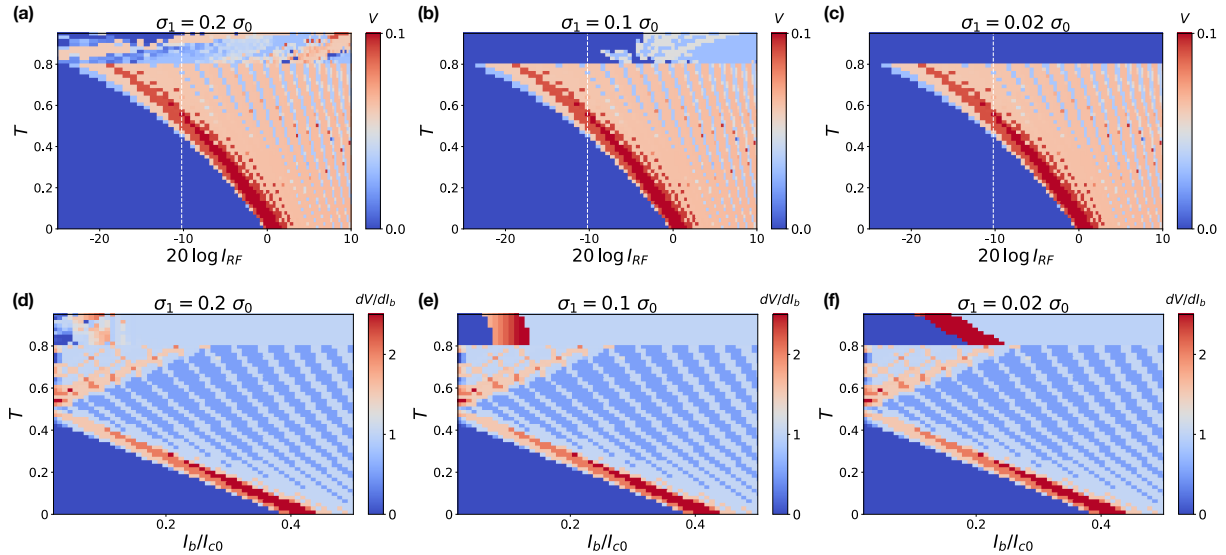


FIG. S2: Exploring reentrance within the RCSJ description, by assuming temperature modified parameters as discussed in the text. The top panels show the case of a small $I_b/I_{c0} = 0.05$. The bottom panels show the case with a fixed $I_{RF}/I_{c0} = 0.6$ (indicated by a dashed white line in the top panels). From left to right the magnitude of abrupt E_C reduction at $T^* = 0.8T_c$ is increased; this is captured by the ratio of σ_1/σ_0 (see text).

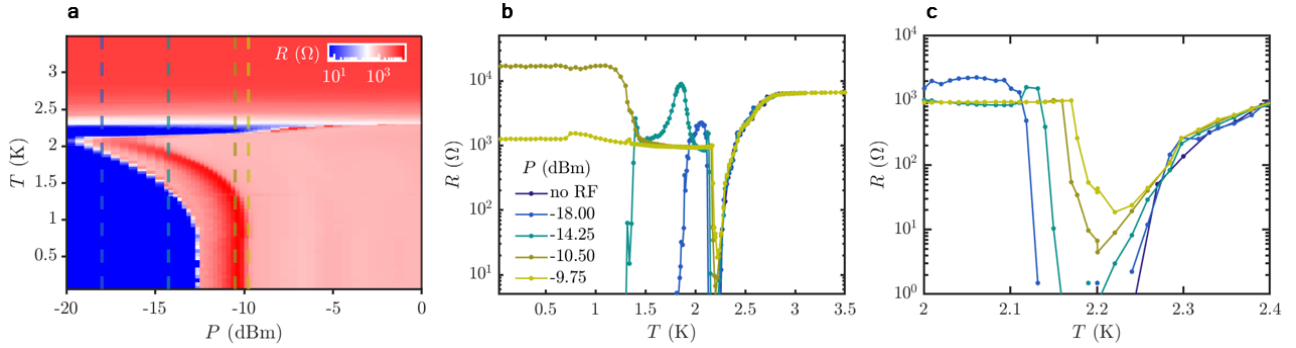


FIG. S3: (a) The $R(T, P)$ phase diagram presented in Fig. 1b in the main text at frequency $f_{\text{RF}} = 24.5$ MHz. (b) $R(T)$ linecuts at selected RF power levels indicated by dashed lines in (a). (c) The $R(T)$ linecuts in the reentrance temperature region SC 2.

V. EXTENDED DATA AND DISCUSSIONS

A. Reentrant superconductivity

To examine the reentrant superconductivity shown in the phase diagram of Fig. 1b in the main text, we analyze five representative line cuts taken at constant power levels, indicated by dashed lines in Fig. S3a. The corresponding resistance versus temperature (R vs. T) curves for each power level are presented in Fig. S3b. A consistent color scheme is used across both figures to denote the different power levels, as referenced to in Fig. S3a. For comparison, we also include the R vs. T trace measured without applied RF power, which exhibits a single superconducting transition at a critical temperature of $T_c = 2.25$ K.

Figure S3c provides a closer view of the $R(T)$ curves in the region where reentrant superconductivity emerges. At $P = -18$ dBm, three distinct transitions are observed: the resistance drops to zero near $T \approx T_c$, rises again at $T = 2.13$ K, and then falls back to zero at $T = 1.8$ K. At a higher power level ($P = -10.5$ dBm), two superconducting transitions are seen, indicating a narrowing of the reentrant region with increasing RF power.

B. The insulating state

1. Estimating the normal state resistance

To estimate the normal-state resistance, we rely on high-current measurements rather than resistance data taken above the superconducting transition temperature (T_c). This is because measurements above T_c include significant contributions from the contact regions, due to the quasi-four-probe configuration of our setup. Instead, we take advantage of the device geometry, which features relatively wide contact regions. As described in Ref. [9], upon increasing the DC current I_b beyond I_c , defined in Fig. S4a, the nanobridge and parts of the contacts switch to the resistive state. When I_b is reduced towards I_r (also defined in Fig. S4a) the contacts return to the superconducting state first, followed by the nanobridge at $I_b = I_r$. Thus we estimate R_N as dV/dI_b obtained right before $I_b = I_r$, where we assume the nanobridge is in the normal state while the contacts are superconducting. While it is possible that parts of the contact pads also remain resistive under these conditions, potentially increasing the measured resistance, we treat this value as an upper bound for the true normal-state resistance. Using this procedure we obtain an upper limit to the normal-state resistance, $R_N = 1.55$ kΩ.

2. Study the temperature dependence of the insulating state

In Fig. S4b we demonstrate that in the insulating (I) state, the resistance follows a sharp exponential rise beyond ten times R_N , then saturates at low temperatures. The observed exponential rise is stronger than that observed for electron localization triggered by Coulomb interactions in insulating granular aluminum films [10]. At low temperatures the resistance saturates close to 50 kΩ. We believe that this saturation is not intrinsic and it is due to the experimental limitations in our measurement system. We demonstrate that in the next paragraph

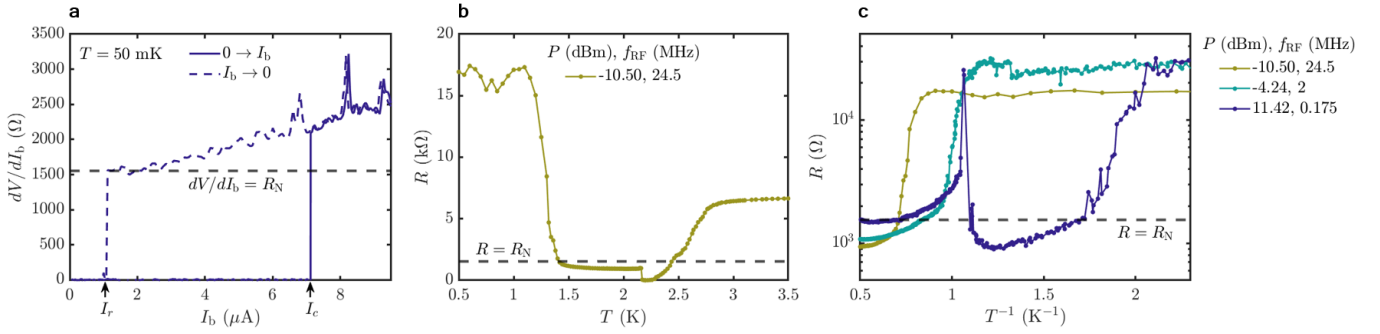


FIG. S4: (a) dV/dI_b (I_b) measured at opposite current sweep directions in the absence of RF power. (b) R (T) measured in the presence of RF power of $P_1 = -10.5$ dBm and $f_{\text{RF}} = 24.5$ MHz, showing the insulating state in comparison to the normal state resistance R_N . (c) Exploration of the RF frequency dependence of the insulating state. R (T) curves are shown for selected RF frequencies and their corresponding input RF powers.

3. Origin of the low temperature saturation

Figure S4c examines the frequency dependence of resistance in the insulating state. For each RF frequency (f_{RF}), we measure resistance (R) as a function of input power (P) at base temperature and identify the power level, $P_1(f_{\text{RF}})$, at which R reaches its maximum. While the actual RF power delivered to the sample may vary with frequency, selecting the peak resistance point allows us to assume that the effective RF power within the device is approximately frequency-independent.

At lower RF frequencies, we observe a lower saturation temperature. One possible explanation is that as the device enters the insulating regime and resistance increases, more power is dissipated, potentially heating the electrons and limiting how cold the electron temperature can get. Another contributing factor may be limitations in our measurement setup, particularly the RF bias tee filters, which include 50 $\text{k}\Omega$ resistors—comparable to the resistance values observed at saturation. These constraints suggest that, in the absence of such limitations, the resistance could have continued to increase with further cooling.

C. Finite voltage width of the giant Shapiro steps

Here we demonstrate that the observed giant Shapiro steps are characterized by a finite voltage width. In Fig. S5a we show dV/dI_b as a function of P and the normalized voltage V/V_0 , at $f_{\text{RF}} = 67.5$ MHz. The voltage V is obtained by integrating the measured dV/dI_b with respect to I_b . $V_0 = 60 \mu\text{V}$ is the typical quantization voltage obtained in Fig. 3b in the main text. As can be seen, the quantized voltage is significantly smeared. The voltage steps are reflected in bright regions in the dV/dI_b color map. In the case of a uniform JJ array, these bright regions should follow straight vertical lines at integer values of V/V_0 (indicated by solid lines in Fig. S5a for comparison). In contrast, here the bright regions form a diagonal pattern, smeared towards non-integer V/V_0 values. This finite voltage width is further demonstrated in Fig. S5b, where we analyze several representative line cuts taken at constant power levels, indicated by dashed lines in Fig. S5a. At $P = -10.7$ dBm, we see a minimum of dV/dI_b at $V/V_0 \simeq 1$, while for $P = -9.5$ dBm this minimum appears at $V/V_0 \simeq 0.5$ due to the smearing. This smearing may result from distribution of junction properties in our naturally occurring JJ array. This disorder, however, may not be sufficient to completely diminish the giant steps observed; therefore, we expect it to be minimal.

D. Absence of RF overheating

The presence of RF power may create dissipation and electron overheating [11]. It appears as a discontinuous jump of $I_{c,\text{eff}}$ with increasing I_{RF} . However, our naturally occurring array is controlled to exhibit negligible overheating as it is tunable at low f_{RF} , since the dissipated power is proportional to f_{RF}^2 . This is evident by the continuous suppression of $I_{c,\text{eff}}$ with increasing P (Fig. 1a) and the absence of hysteresis of R over P sweeps for frequencies $f_{\text{RF}} < 25$ MHz (not shown). This contrasts with operation at high frequencies, where the discontinuity is visible, as can be seen in Fig 3c in the main text for $f_{\text{RF}} = 67.5$ MHz. Therefore, we suggest that the observed superconductor-to-insulator

transition and reentrant superconductivity can be interpreted in the regime of negligible overheating.

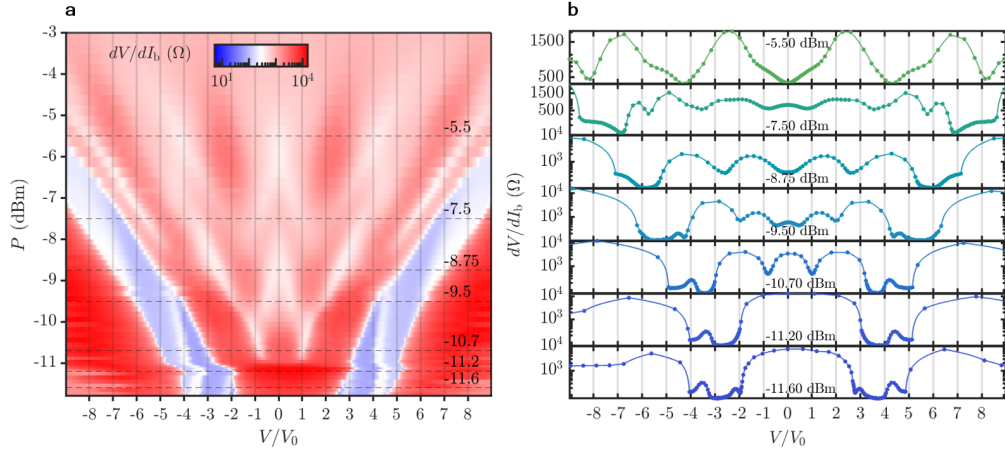


FIG. S5: (a) dV/dI_b as a function of V/V_0 and P at $f_{\text{RF}} = 67.5$ MHz, where $V_0 = 60$ μ V. (b) dV/dI_b vs. V/V_0 curves obtained at constant power levels indicated by dashed lines in (a).

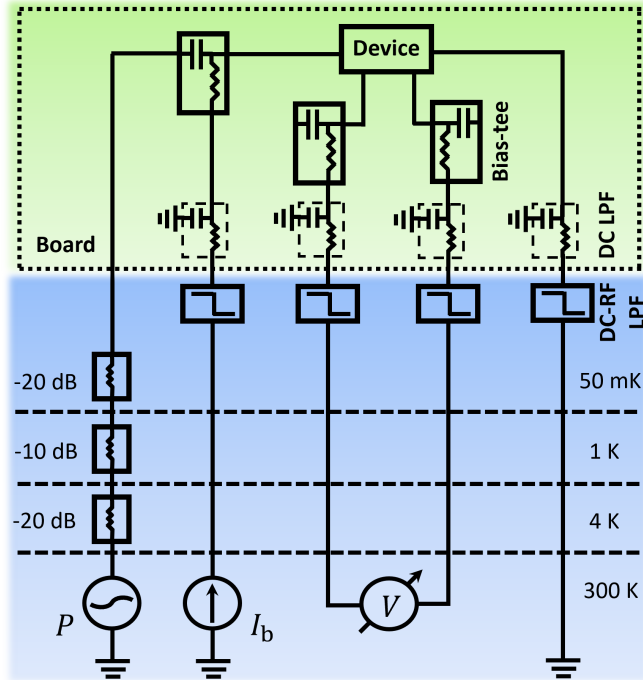


FIG. S6: The measurement setup used in the experiment.

[1] J. Koch, T. M. Yu, J. Gambetta, A. A. Houck, D. I. Schuster, J. Majer, A. Blais, M. H. Devoret, S. M. Girvin, and R. J. Schoelkopf, Charge-insensitive qubit design derived from the cooper pair box, *Phys. Rev. A* **76**, 042319 (2007).

[2] K. K. Likharev and A. B. Zorin, Theory of the bloch-wave oscillations in small josephson junctions, *Journal of Low Temperature Physics* **59**, 347 (1985).

[3] J. S. Penttilä, U. Parts, P. J. Hakonen, M. A. Paalanen, and E. B. Sonin, “superconductor-insulator transition” in a single josephson junction, *Phys. Rev. Lett.* **82**, 1004 (1999).

[4] Y. Takahide, R. Yagi, A. Kanda, Y. Ootuka, and S.-i. Kobayashi, Superconductor-insulator transition in a two-dimensional array of resistively shunted small josephson junctions, *Phys. Rev. Lett.* **85**, 1974 (2000).

- [5] A. Gómez-León and G. Platero, Floquet-bloch theory and topology in periodically driven lattices, *Phys. Rev. Lett.* **110**, 200403 (2013).
- [6] F. Grossmann, T. Dittrich, P. Jung, and P. Hänggi, Coherent destruction of tunneling, *Phys. Rev. Lett.* **67**, 516 (1991).
- [7] K. Ravindran, L. Gómez, R. Li, S. Herbert, P. Lukens, Y. Jun, S. Elhamri, R. Newrock, and D. Mast, Frequency dependence of giant shapiro steps in ordered and site-disordered proximity-coupled josephson-junction arrays, *Phys. Rev. B* **53**, 5141 (1996).
- [8] K. Efetov, Phase transition in granulated superconductors, *Sov. Phys.-JETP (Engl. Transl.);(United States)* **51** (1980).
- [9] D. Hazra, J. R. Kirtley, and K. Hasselbach, Retrapping current in bridge-type nano-squids, *Phys. Rev. Appl.* **4**, 024021 (2015).
- [10] G. Deutscher, B. Bandyopadhyay, T. Chui, P. Lindenfeld, W. L. McLean, and T. Worthington, Transition to localization in granular aluminum films, *Phys. Rev. Lett.* **44**, 1150 (1980).
- [11] A. D. Cecco, K. L. Calvez, B. Sacépé, C. B. Winkelmann, and H. Courtois, Interplay between electron overheating and ac josephson effect, *Phys. Rev. B* **93**, 180505 (2016).